

*Proceedings of the Korean Nuclear Society Autumn Meeting
Seoul, Korea, October 2001*

Scaling and Parametric Studies of Condensation Oscillation in an In-containment Refueling Water Storage Tank

Jun Hyung Lee* and Hee Cheon NO**

**Korea Power Engineering Company*

***Korea Advanced Institute of Science and Technology*

Abstract

The purpose of this paper is to study the condensation oscillation phenomena by steam-jetting into subcooled water through a sparger, implementing a scaling methodology and the similarity correlation between the test facility and model prototype. In addition, the results of this study can provide suitable guidelines for sparger design utilized in the IRWST for the Advanced Passive Reactor 1400 (APR1400). To corroborate the scaling methodology, various experimental tests were conducted. The scaling-related parameters experimentally considered were water temperatures, mass flux, discharge system volumes, tank sizes, source pressure, steam-jetting directions, and numbers of sparger discharge holes. To preserve the scaling similarity, the thickness of the minimum water volume created by the boundary layer that encloses the steam cavity was found to be equal to the maximum length of the steam cavity formed. Four key scaling parameters were identified and empirically correlated with the maximum amplitude of pressure oscillation. They are as follows: Volume of the steam cavity, flow restriction coefficient, discharge hole area, and density ratio of steam to water. Variations of the oscillation amplitude were small when steam-jetting directions were altered. The concept of a reduction factor was introduced for estimating the oscillation amplitude of the multi-hole sparger with test data from a single-hole sparger.

1. Introduction

An In-containment Refueling Water Storage Tank (IRWST) is used as a passive safety feature for the Advanced Passive Reactor 1400 (APR1400). When the Safety Depressurization & Vent System (SDVS) is actuated, the reactor is rapidly depressurized and the reactor coolant is discharged into the IRWST. The IRWST water temperature rises as depressurization occurs. As steam is discharged, the condensation oscillation occurs in the IRWST, which causes pressure oscillation to intensify as the water temperature rises to a certain level and then rapidly declines thereafter. If a discharge device is not properly designed, the structural integrity of a tank may be impaired when severe oscillation loads are imposed on its boundary ⁽¹⁾. Appropriate design guidelines for a multi-hole sparger and tank are needed to avoid structural failures.

Several authors have identified the major role of water temperature plays in the variation of pressure oscillation. Utamura (1986) introduced a physical model to explain the mechanism of condensation oscillation. In this model, entrained liquid droplets within the steam cavity are assumed to control condensation heat transfer rate. Utamura also introduced an oscillation amplitude correlation by use of dimensionless parameters such as subcooling, discharge hole diameters, and steam velocities. Aya and Nariai (1983) qualitatively defined the difference between chugging and the condensation oscillation phenomena. Aya and Nariai showed that a

period of the steam-water interface behavior coincided with that of pressure oscillation time histories. Sonin and Chun (1983) developed a similarity methodology for a small-scale steam discharge system that was geometrically proportional to a full-scale prototype. They investigated different discharge hole configurations and found that a specific multi-hole sparger reduced the amplitude of pressure oscillation by a factor of eight when compared to a single-hole sparger with equivalent area and mass flux. Damasio (1985) developed a correlation for oscillation frequencies as a function of steam velocity, water temperature, and discharge hole diameter. Oscillation frequency increases as mass flux increases and decreases as water temperatures rise. In addition, oscillation frequency is inversely affected by the discharge hole diameter.

Three major topics are introduced in this study. First, a scaling methodology is developed for the SDVS, the IRWST, and the steam cavity, thereby, establishing the scaling numbers that are derived from the governing equations. In addition, to corroborate the scaling methodology, experimental tests to measure time histories of pressure oscillation are performed. Consequently, the relationships between the scaling and experimental parameters are verified. Second, from the scaling methodology and its corroboration, key scaling parameters are revealed and are used as the basis for correlating empirical data. Thereby, a method of estimating the maximum oscillation amplitude of a prototype sparger can be determined.

2. Scaling Methodology of Condensation Oscillation Phenomena

Test facilities are subdivided into two major systems: the steam discharge system and the tank system. The steam discharge system consists of steam generating, pipe run, and steam cavity regions. The pipe run region is from the exit of steam generator to the steam discharge hole. After the pipe run region, steam-jetting forms the steam cavity. Since the energy change from the steam-generating region to the discharge hole exit is negligible, the energy equation can be ignored. The scaling of the tank system uses the energy equation as the governing equation and provides one scaling parameter as the tank size. A typical system under consideration is illustrated in Figure 3.1.

The scaling of the momentum is performed with two objectives: one is the geometrical effect on condensation oscillation for the test facility and the other is the oscillation behavior of the steam cavity.

2.1 Scaling of test facility

2.1.1 Steam discharge system

The nondimensionalized mass conservation equation at the steam-generating region is

$$\text{Steam generator: } N_{\tau S/G} \cdot \frac{d(\rho_s^* V_{S/G}^*)}{dt^*} = -W_{S/G in}^* + \frac{Q_{input}^*}{h_{fg}^*} \quad (2.1)$$

with the following nondimensional variables:

$$W_{S/G in}^* = \frac{W_{S/G in}}{W_o}, \quad Q_{input}^* = \frac{Q_{input}}{Q_{input o}}, \quad h_{fg}^* = \frac{h_{fg}}{h_{fg o}}, \quad \rho_s^* = \frac{\rho_s}{\rho_{s o}}, \quad V_{S/G}^* = \frac{V_{S/G}}{V_o}, \quad t^* = \frac{t}{\tau_o}$$

and $\tau_o = \frac{\rho_s V_{sc}}{W_o}$.

Similar equations, shown below, of the pipe run and the steam cavity regions are derived:

o *Pipe run*: $N_{\tau_{pipe}} \cdot \frac{d(\rho_s^* V_{pipe}^*)}{dt^*} = \frac{1}{N_1} W_{pipe\ in}^* - W_{pipe\ out}^*$, (2.2)

o *Steam cavity*: $N_{\tau_{sc}} \cdot \frac{d(\rho_s^* V_{sc}^*)}{dt^*} = \frac{W_{pipe\ out}^*}{N_2 N_3} - W_c^*$. (2.3)

where the denominators, N_1 , N_2 , and N_3 represent the total number of pipe runs, spargers, and discharge holes, respectively. Each scaling number is a ratio of the regional transport time constant to the characteristic time constant of the steady state:

$$N_{\tau_{S/G}} = \frac{\tau_{S/G}}{\tau_o}, \quad N_{\tau_{pipe}} = \frac{\tau_{pipe}}{\tau_o}, \quad \text{and} \quad N_{\tau_{sc}} = \frac{\tau_{sc}}{\tau_o}.$$

By the scaling of the test facility, the physical dimensions that would simulate the condensation oscillation behavior of a prototype can be determined. Table 2.1 shows the scaling ratios of the test facility.

2.1.2 Tank system

We can write the nondimensionalized energy equation of the tank as

$$\frac{de_{tank}}{dt} = W_c h_{fg} - W_{evaporative} h_{fg} - Q_{loss} \quad (2.4)$$

$$\left(\frac{\rho_f V_{minimum}}{W_o \tau_{tank}} \right) \cdot \frac{\tau_{tank}}{\tau_o} \cdot \frac{d(e_{tank}^*)}{dt^*} = W_c^* h_{fg}^* - W_{evaporative}^* h_{fg}^* - \frac{Q_{loss}}{W_o \Delta h_o}, \quad (2.5)$$

where $\tau_{tank} = \frac{\rho_f V_{minimum}}{W_o}$.

The last two terms on the right hand side represent evaporative and heat losses from the tank. The minimum water volume, $V_{minimum}$, is a minimum volume of water tank to preserve the shape and the scaling similarity of the steam cavity.

$$N_{\tau_{tank}} = \frac{\tau_{tank}}{\tau_o} = \frac{\rho_f}{\rho_s} \cdot \frac{V_{minimum}}{V_o} : \text{Energy time-constant number.}$$

2.2 Scaling of momentum

2.2.1 Integral momentum of test facility

The integral momentum equation from the steam generating to the steam cavity regions is

$$\frac{d(\rho u V)_s}{dt} + [(A \rho u^2)_s]_{in}^{out} + A [P]_{in}^{out} = \int_{V_s} [\Gamma u_s - F_i - F_{friction}] dV . \quad (2.6)$$

The nondimensionalized form of Equation (2.6) is

$$\begin{aligned} & \left[\frac{IW_o}{\tau_m^{integral} \rho_s u_s^2} \right] \cdot \frac{\tau_m^{integral}}{\tau_o} \cdot \frac{dW_o^*}{dt^*} + \left[\frac{W_o^{*2}}{\rho_s^* A^{*2}} \right]_{in}^{out} + \frac{\delta P_o}{\rho_s u_s^2} [P^*]_{in}^{out} \\ & = - \left[\sum_j \frac{f_j L_j}{D_{hj}} + \sum_j K_k \right] \cdot \frac{(\rho_s^* u_s^{*2})^2}{2} - f_i \cdot \frac{\rho_s^* u_s^{*2}}{2} + \frac{W_c^* u_s^*}{A_{sc}^*} \end{aligned} \quad (2.7)$$

where $\tau_m^{integral} = \frac{IW_o}{\rho_s u_s^2}$.

$$N_{\tau_m^{integral}} = \frac{\tau_m^{integral}}{\tau_o} = \frac{(IV_{system}/u_s^2)}{(\rho_s V_{sc}/W_o)} : \text{Integral time constant number}$$

$$N_P = \frac{\delta P_o}{\rho_s u_s^2} = \frac{(P_{source} - P_{tank})}{\rho_s u_s^2} : \text{Source pressure number}$$

$$N_{K_f} = \sum_j \frac{f_j L_j}{D_{hj}} + \sum_j (K_k)_j : \text{Friction and form number}$$

2.2.2 Oscillation momentum of steam cavity

The momentum equation for the oscillatory steam cavity is derived with an assumption of the spherical shape of the steam cavity:

$$\begin{aligned} & \frac{\rho_f V_{sc}^{2/3}}{(\tau_m^{sc})^2 \cdot \rho_s u_s^2} \cdot \left[R_{sc}^* \frac{d^2 R_{sc}^*}{dt^{*2}} + \frac{3}{2} \cdot \left(\frac{dR_{sc}^*}{dt^*} \right)^2 \right] \\ & = \frac{\delta P_o}{\rho_s u_s^2} [P_{source} - P_{tank}] - \frac{\rho_f g L_{zo}}{\rho_s u_s^2} \cdot [H_i^* - z^*] - \left[\sum_j \frac{f_j L_j}{D_{hj}} + \sum_j (K_k)_j \right] \cdot \frac{\rho_s^* u_s^{*2}}{2} \end{aligned} \quad (2.8)$$

where $\tau_m^{sc} = \left(\frac{\rho_f}{\rho_s} \right)^{1/2} \cdot \frac{V_{sc}^{1/3}}{u_s}$.

$$N_{submersion} = \frac{\rho_f g L_{zo}}{\rho_s u_s^2} : \text{Submersion number}$$

$$N_{\tau_m^{sc}} = \left(\frac{\rho_f}{\rho_s} \right)^{1/2} \cdot \left(\frac{V_{sc}^{1/3}}{L_{sc}} \right) : \text{Steam cavity time-constant number.}$$

2.3 Summary of the scaling methodology

Each scaled property is represented by coefficients of the nondimensionalized governing equations and is generally expressed as ϕ .

$$\phi_R = \frac{\phi_{for\ model}}{\phi_{for\ prototype}} . \quad (2.9)$$

In order to design a scaled test facility and to simulate the dynamic behavior of the steam

cavity, the similarity criteria from the scaling methodology must be satisfied.

The results of the scaling methodology and the scaling parameters are shown in Table 2.2. The outcome of this methodology is a set of characteristic time constants and the similarity criteria. If we set V_o to V_{sc} , and simulate a single hole of the multi-hole sparger during testing, then the characteristic time constant from the steam cavity mass conservation equation then becomes unity and is shown in Table 2.2. The other characteristic time constants from the mass conservation equations of the steam generator and the pipe run regions can be determined by replacing V_o with V_{sc} . The time constant scaling parameters from the momentum and energy equations can also be determined by substituting V_o for V_{sc} . If the density ratio of the model is the same as the prototype, the similarity requirement for the energy time-constant number provides the volume ratio of the minimum water to the steam cavity.

By use of the scaling numbers, a general integral equation of the nondimensionalized oscillation pressure is established.

$$P_{sc}^* = \int_0^{t^*} f(N_{\tau_{SG}}, N_{\tau_{pipe}}, N_{\tau_{sc}}, N_m^{integral}, N_m^{sc}, N_{submersion}, N_{P_o}, N_{K_f}, N_{\tau_{tank}}, N_{heat\ loss}) dt^* \quad (2.10)$$

$$\text{where } t^* = \frac{t}{\tau_o} \text{ and } P_{sc}^* = \frac{P_{sc}}{P_o}.$$

3. Corroborating the Scaling Methodology

The purpose of this experiment is to identify parameters known to affect the condensation oscillation phenomena and to corroborate the scaling methodology. The steam generator is filled from an external supply of demineralized water, which is heated and then released as steam at a maximum pressure of 440kPa. The steam flow rate is controlled by means of a pneumatic actuated control valve. The entire steam discharge piping is insulated with 1-inch asbestos. Prior to the steam ejection into the test water tank, a moisture separator is installed upstream to remove additional suspended liquid droplets. Two piezoelectric pressure transducers are installed at the side shell and the bottom plate of the test water tank to measure pressure time histories. The two piezoelectric pressure transducers are flush-mounted on the tank. These transducers have high sensitivity and acceleration compensated ICP quartz pressure sensors suitable for measuring low-pressure acoustic impulses in a hydraulic and/or pneumatic system. They have unique capabilities to measure pressure changes as low as 6.895 Pa under high static conditions. They have a sensitivity of 0.04mV/Pa and a resolution of 91dB (0.689 Pa) at a typical sampling rate of 10k per second. Bulk water temperatures are monitored with T-type thermocouples. These T-type thermocouples are installed in the side of the test tank so that the thermocouples protrude 50mm into the tank. Average values from the four thermocouple readings are used as bulk water temperatures. Temperature profiles of the steam cavity and the surrounding liquid fields are measured by an instrument bar containing ten thermocouples inserted linearly at 20mm intervals. Oscillatory behaviors of the steam cavity are photographed with a high-speed video camera. Utilizing the instrument bar the length of the steam cavity is also measured.

Figure 3.1 shows the instrument bar and the schematic diagram of the test facility that correlates with the scaling methodology. Test matrixes of steam-jetting via the single- and multi-hole spargers are shown in Tables 3.1 and 3.2, respectively.

3.1 Experimental parameters

When the steam is ejected into the subcooled water, a steam cavity is formed as shown in Figure 3.2. According to the mass flux at a given source pressure, the oscillatory behavior of the steam cavity results in distinct patterns. In a subsonic steam jet, two kinds of inertia produce the steam-water interface to reciprocate. After the steam cavity is initially formed, the water inertia forces the steam cavity to retract. After the steam cavity retraction, outgoing steam mass flux induces the steam cavity to over-expand. After over-expanding, the condensation rate on its interface increases the outgoing steam mass flux and as a result, the steam cavity will retract. Analyzing the steam cavity from the photographed pictures, the amplitude of the reciprocating motion is almost same as the square root of the discharge hole diameter.

However, flow inertia of a sonic steam jet is sufficiently high to maintain the steam cavity shape as if no water inertia existed. From the tests, the threshold mass flux of the sonic steam jet is found to be $200 \text{ kg/m}^2\text{sec}$. Figures 3.3 and 3.4 show the pressure time histories and FFT results of the subsonic ($Q=150 \text{ kg/m}^2\text{sec}$) and sonic ($Q=400 \text{ kg/m}^2\text{sec}$) steam jets. For both the subsonic and sonic steam jets, the pressure time histories correspond to oscillatory motion of the steam cavity ⁽²⁾⁽⁴⁾.

When determining the dominant frequency, series of repetitive tests with various ranges of frequencies are conducted and the repetitive maximum peak value of the FFT is utilized. If the FFT does not indicate a maximum peak and shows widened oscillation frequency values, then the averaged value of the oscillation frequency components is utilized as the dominant frequency.

As the water temperature rises, the condensation capability of water diminishes and the steam cavity grows. The oscillation amplitude increases up to a water temperature of 80°C , which is defined as an unstable condensation temperature, and rapidly decreases thereafter. As the water temperature exceeds the unstable condensation temperature, the condensation capability of water becomes negligible. In addition, the size of the steam cavity rapidly increases and bubbling of the steam cavity begins to occur. A larger steam cavity produces lower oscillation frequency. Up to the unstable condensation temperature, the oscillation amplitude is greatly influenced by the size of the steam cavity. However, once the water temperature exceeds the unstable condensation temperature, the oscillation amplitude is greatly influenced by the lowered oscillation frequency.

3.1.1 Single-hole sparger

o *Water temperature*: The reciprocating behavior of the steam cavity that occurs at the subsonic steam jet quakes the surrounding water mass and produces higher oscillation amplitude than that of the sonic steam jet. However, at a water temperature of 30°C , the almost instantaneous mass balance between the incoming steam mass flow rate and the condensate rate causes the very small amplitude of the steam cavity oscillation at the sonic steam jet.

Above the water temperature of 80°C , the ejected steam cannot be completely condensed. The condensation capability of water at a low temperature is unlimited and, thus the liquid inertia controls the collapse of the steam cavity. Contrarily, condensation heat transfer controls the collapse of the steam cavity at high water temperatures ⁽⁶⁾. At the unstable condensation temperature, the capability of condensing steam is small. During the process of collapsing, condensing capability is lost and the steam cavity is compressed adiabatically. (?)Continual steam-jetting creates an elongated steam cavity until a large interfacial area for condensation is achieved. The surface of the steam cavity becomes wide and bulgy. The steam cavity oscillates turbulently both in subsonic and sonic steam jets, which create violent swelling of the water

surface during the tests. It is presumed that rapid condensation is triggered by cold eddy near the enlarged steam-water interface leading to anomalous and turbulent oscillatory behavior of the steam cavity near the unstable oscillation temperature.

When the water temperature reaches 90°C, bubbling temperature, water has negligible condensation capability. The steam cavity elongates and separately forms steam bubbles. These steam bubbles slowly rise to the surface of the water. A mass flux of the subsonic steam jet is not sufficiently high to induce pressure oscillation, which causes the steam cavity to break into several large steam bubbles. As the mass flux increases, the size of the steam bubbles becomes asymptotically smaller. A concentrated swarm of fine steam bubbles is developed and is broken up by the strong turbulence of water just after the separation ⁽⁷⁾. This is called a detachment and fragmentation of steam bubbles. The pressure time history of 400kg/m²sec at a water temperature of 90°C in Figure 3.3 represents pressure oscillation resulting from the detachment and fragmentation.

o *Mass flux*: Figure 3.5 shows the length of the steam cavity with respect to water temperatures. The length of the steam cavity is proportional to the mass flux. In the sonic steam jet, the length of the steam cavity gives a fixed value of 70mm in low water temperatures ranging from 30°C to 50°C. As the temperature rises up to the unstable condensation temperature, the length of the steam cavity deviates from the fixed value. The steam pressure just before the discharge hole exit is lower than the pressure in the steam generator due to friction and form losses. It is assumed that the turbulent oscillatory behavior of the steam cavity at the unstable condensation temperature produces enough oscillatory pressures to disturb the choked condition at the discharge hole exit. Figure 3.6 shows the transition of the oscillation amplitudes with varying mass flux when using the same experimental parameters.

o *Increased Volume*: To see the influence of increased discharge system volume on the oscillation amplitude, two different volumes of drywells, as shown in Figure 3.7 are connected separately with two different pipe run locations: one is 1.5 meters and the other is 12.89 meters from the discharge hole exit.

Figures 3.8 shows the oscillation amplitude of the subsonic steam jet tested for the 1.5 meters connection. According to the connection of the dry well, the oscillation amplitude decreases. Inverted triangle symbols show the amplitude of pressure signals within the drywell. The drywell greatly increases the form loss of the steam discharge system and acts just like a steam-jetting source with highly reduced pressure. The shortened discharge pipe, which is from the dry well to the discharge hole exit has less flow inertia than the discharge pipe without the drywell. As the drywell volume increases, the oscillation amplitude decreases. The drywell near the steam generator (12.89 meters) provides a steam discharge system with a larger mass of steam after the dry well than the dry well far away from the steam generator does. As such, the drywell has no effect on decreasing the oscillation amplitude. The oscillation amplitude of the sonic steam jet hardly varies regardless of sizes and locations of the drywells because the choking takes place at the end of the pipe. The negligible amplitude of pressure signals within the drywell means that it functions as a damper of pressure oscillation. It is noticeable that the turbulent oscillatory behavior of the steam cavity at the unstable condensation temperature is supposed to perturb the choking condition at the discharge hole exit. The oscillation amplitude slightly decreases.(?) Figure 3.9 shows the test results of the sonic steam jets for the 1.5 meters drywell connection.

o *Discharge hole*: For a given mass flux and water temperature, a larger discharge hole produces larger steam cavities and higher oscillation amplitudes. The oscillation frequency is inversely proportional to the diameter of discharge hole ⁽⁵⁾⁽⁸⁾⁽⁹⁾.

o *Minimum water volume*: Smaller water volumes can be obtained by inserting a partition plate into the tank. The partition plate is manufactured to have variable area in order to isolate the rest of the tank water volume. When the steam is ejected in the downward direction, the partition plate is moved perpendicularly to the steam-jetting direction. As the partition plate becomes closer to the steam cavity, the oscillation amplitude and the size of the steam cavity abruptly increase. The minimum water volume, V_{minimum} , enclosing the steam cavity should be secured to preserve the shape and the scaling similarity of the steam cavity. The thickness of the minimum water volume is defined as a layer thickness and is almost equal to the maximum length of the steam cavity formed. A single-hole sparger with a diameter of 15.8 mm has a maximum steam cavity length of 185 mm. When the partition plate remains at a greater distance from the steam cavity than this layer thickness, the oscillation amplitude shows no difference. The test result of the minimum water volume is shown in Figure 3.10. Temperature gradients throughout the layer thickness are found to be 3°C and no more than 1°C higher than bulk water temperatures. Judging from the small temperature gradient, condensation oscillation occurs within a limited volume of tank water.

o *Source pressure*: Generally, higher steam source pressure gives higher mass flux at the constant system friction and form losses. Constant mass flux at an elevated source pressure condition can be obtained by increasing system form losses. By closing the pneumatic actuated control valve during the tests, system form loss increases. Figure 3.11 shows the effect of different source pressure conditions under the same mass flux. The source pressure increased 1.4 times in the subsonic steam jet and approximately 2 times in the sonic steam jet. However, the increase rates of the averaged oscillation amplitudes become 20% in the subsonic steam jet and 10% in the sonic steam jet. It is concluded that the source pressure effect on the oscillation amplitude given the steam mass flux is relatively small and the source pressure effect of the subsonic steam jet is greater than that of the sonic steam jet.

o *Distilled and process water*: The oscillation amplitude becomes higher when degassed water is used as a condensing agent. Figure 3.12 shows the difference of the oscillation amplitude when either distilled or process water is used. This discrepancy arises because noncondensable gasses in the process water act as a dampening medium. According to the temperature rise, noncondensable gas disappears and the difference in the oscillation amplitude becomes negligible.

o *Directional effect*: Regardless of change in the orientation of the measurement and steam-jetting direction, the oscillation amplitudes measured at the bottom plate and the side shell of the tank produce no clear difference.

3.1.2 Multi-hole sparger

By comparing the oscillation amplitude of the multi-hole sparger with that of the equivalent single-hole, the performance and usefulness of the multi-hole sparger can be indicated. Figure 3.13 shows the oscillation amplitudes of 1- ϕ 10mm, 4- ϕ 5mm, and 1- ϕ 5mm spargers, respectively. The oscillation amplitude of the 1- ϕ 10mm equivalent single-hole sparger is lowered by use of the 4- ϕ 5mm multi-hole sparger. This is because the 4- ϕ 5mm multi-hole sparger produces smaller steam cavities. It is noticeable that the maximum oscillation amplitudes of the 2- ϕ 5mm and 4- ϕ 5mm spargers are 1.4 and 1.5 times higher than those of the expected two and four times of the 1- ϕ 5mm single hole sparger. The oscillation amplitude resulting from one steam cavity may be attenuated by adjacent steam cavities. With an increase of the number of holes, one may assume that the attenuation will be more enhanced. Figure 3.14 shows the multiplication factor when increasing the number of holes under the same mass

flux.

At the unstable condensation temperature, there are different frequency components of the equivalent single-hole sparger. It is assumed that the turbulent oscillatory behavior of the steam cavity is unequally distributed throughout the steam-water interface. This may cause locally non-synchronous and irregular oscillatory behavior of the steam cavity. However, in the vicinity of the multi-hole sparger, where the steam-water interface is torn and formed, the multi-hole sparger cannot form steam cavities as large as those made by the equivalent single-hole sparger. The mass flux at a given source pressure equally distributed before steam ejected. The oscillation frequency via the multi-hole sparger produces a constant value. Figure 3.15 shows the different frequency components of each sparger type. The frequency with the multi-hole sparger is higher at low temperature and lower at high temperature than that with an equivalent single hole.

o Directional effect: Influences of the different steam jetting directions of sparger holes on the oscillation amplitude are examined under the same mass flux with the 4- ϕ 5mm multi-hole sparger. The 4- ϕ 5mm multi-hole sparger is installed in such a way that the steam jets in the horizontal and downward directions for four separate cases: the first case has the steam-jetting from the four sparger holes towards the pressure transducer on the tank boundary, ; the second case represents the sparger rotated 180°, ; the third case presents three holes horizontally and the other hole in the downward direction, ;and, finally, in the fourth case each one of the four sparger holes ejects 90° apart in all four directions. In the first and second cases, the distance between holes is 10 millimeters from center to center. Figure 3.16 shows the oscillation amplitude of each sparger test case. In each sparger test case, the oscillation amplitudes show no great difference from the different jetting directions. It is concluded that the jetting directions of the holes are of negligible influence.

o Reduction factor: In order to observe the effect of the number of holes, two different multi-hole spargers are used. One has 4 holes with diameters of 5mm and the other has 10 holes with diameters of 3.16mm. These two multi-hole spargers have the same discharge area as the 1- ϕ 10mm equivalent single-hole sparger has. Figure 3.17 shows the result of increasing the number of holes. A reduction factor is defined as the oscillation amplitude ratio of the multi-hole sparger to that of the equivalent single-hole sparger. As the number of holes increases, the maximum oscillation amplitude and the reduction factor decrease. In a mass flux of 400 kg/m²sec, the reduction factor of the 4- ϕ 5mm and the 10- ϕ 3.16mm multi-hole spargers are 0.7 and 0.23, respectively. It is presumed that further increase of the number of holes eventually saturates makes the reduction factor and this saturated reduction factor decreases with an increase of the mass flux. Increases in the number of holes are four and ten times than that of the 1- ϕ 10mm equivalent single-hole sparger. However, the diameters of one hole of each multi-hole sparger decrease to one-half and approximately one-third times that of the 1- ϕ 10mm equivalent single-hole sparger. It is recognized that the decrease rate of the oscillation amplitude is more susceptible to one hole having a smaller diameter than the augmented number of holes.

o Minimum water volume: It is obvious that the oscillation amplitude via the multi-hole sparger steam jetting increased as the steam cavities become closer to the structural boundary. The layer thickness created formed by the 1- ϕ 5mm single-hole sparger steam-jetting was found to be 90 mm. Four holes of the 4- ϕ 5mm multi-hole sparger were lined up with 10mm clearance. Apparently, the steam cavities and those layer thickness overlap each other. This interference effect lengthens the steam cavities slightly. Figure 3.18 shows the effect of the minimum water volume. The oscillation amplitude begins to slightly increase at a distance of 120 mm, which can be defined as the layer thickness of the 4- ϕ 5mm multi-hole sparger.

4. Scaling Evaluation and Oscillation Amplitude Correlation

4.1 Scaling evaluation

With regard to the quantitative results of this study, the importance of each scaling parameter was revealed and the similarity requirements were assessed. If the minimum water volume is not impeded by structural boundaries, the time constant scaling parameter from the energy time constant number becomes negligible. The time constant scaling parameters from the integral momentum equation are the volume ratio of the steam discharge system and the steam cavity. From the increased discharge system volume test results, the drywell connected near the exit of the sparger acts just like a steam-jetting source with highly reduced pressure and makes it possible to ignore the physical configuration of the upstream discharge system volume. Actually, the SDVS pipe has a drywell just before discharge holes. Thereby, the system volume as the time constant scaling parameter is negligible.

The scaling requirements for the source pressure number and the submersion number can be satisfied as follows: Long-term depressurization of the SDVS is assumed to occur at highly reduced source pressure that is well within the capability of the test conditions. If we consider the saturation pressure and temperature in the test to the same properties in a full pressure prototype, the fluid properties exhibit self-similarity over the tested conditions and the scaling requirement for the source pressure number is maintained operationally. If sufficient submersion is provided, the submersion depth of the discharge pipe exerts little influence on the oscillation amplitude ⁽⁴⁾ and the scaling requirement for the submersion number is fairly satisfied.

Table 4.1 shows the effects on the oscillation amplitude for the experimental parameters and those implications in the scaling parameters. Some scaling parameters become important when the steam-jetting occurs at the subsonic steam jet and are ranked as medium. From the results of the scaling evaluation, the same condensation oscillation phenomena occur in the scaled-down experimental facility as may be expected in the IRWST.

4.2 Oscillation amplitude for single-hole sparger

By use of the key scaling parameters and the assessment results of the similarity requirements, the oscillation amplitude at the unstable condensation temperature is empirically correlated in terms of discharge hole area, density ratio of source steam to liquid, steam cavity volume, and system friction and form losses. Equation (4.1) is also a simplified form of the general integral equation of oscillation pressure as shown in Equation (2.10).

$$\frac{\Delta P}{P_o} = 4.157 * 10^6 \cdot K_f^{-0.774} \left(\frac{A_{hole}}{V_{sc}^{2/3}} \right)^{1.771} \left(\frac{\rho_f}{\rho_s} \right)^{-2.101} \quad (4.1)$$

where P_o is the atmospheric pressure. Pressure difference as the numerator of the source pressure number, N_{p_o} , in equation (2.10) gives pressure of the steam generator as a variable. Pressure at the outside of the discharge exit is assumed to be constant and the density of source steam as the scaling parameter directly depends on the pressure of the steam generator. We can use the density of source steam as a variable in Equation (4.1), instead of the source pressure number for simplification. The density of source steam not only embraces the source pressure number but also dominates the mass flux. Therefore, the ratio of density represents the effect of the steam mass flux on the oscillation pressure. The density of water is calculated at the bulk water temperatures. Discharge hole diameters (5, 10, and 15.8 mm) as experimental parameters

are changed in accordance with varying steam mass fluxes from 70 to 400 kg/m²sec. Assuming the geometrical configuration of the steam cavity in the subsonic steam jet is a hemisphere, its volume is obtained from the measured length of the steam cavity. In the sonic steam jet, the contour of the steam cavity is assumed to be a second polynomial and partially integrated from the tip of the steam cavity to the discharge hole exit. With increases of discharge hole area and source steam density, the oscillation amplitude increases. However, a flow restriction coefficient that consists of friction and form losses adversely affects the oscillation amplitude. The test results with the correlated maximum oscillation amplitude are shown in Figure 4.1. The variables in Equation (4.1) are all known quantities except the steam cavity length. In order to correlate the steam cavity length data with definable variables, three dimensionless numbers are employed.

$$\frac{L_{cavity}}{D_{hole}} = 11.79 \cdot Re^{-0.364} Ja^{-0.564} We^{0.597} . \quad (4.2)$$

The steam cavity length data ranging from 60 to 90°C were used in the correlation of Equation (4.2). Figure 4.2 shows the results of the correlation. The Reynolds number governs the rate of heat transport and is inversely proportional to the length of the steam cavity. The Jacob number represents the condensation capability of the water and the energy density of the steam. To consider the formation of the steam cavity at a given mass flux, the Weber number is introduced. This tendency for those dimensionless numbers to delineate the behavior of the steam cavity length agrees well with the previous result ⁽⁵⁾ and with physical insight.

4.3 Oscillation amplitude for multi-hole sparger

The key scaling parameters used in equation (4.1) were selected by utilizing basic equations simulating the behavior of one steam cavity. The test results of the multi-hole sparger showed that the oscillatory behavior of one steam cavity is interfered by adjacent steam cavities. In order to consider the interference effect among the steam cavities and to estimate the maximum oscillation amplitude of a prototype multi-hole sparger, the reduction factor was introduced. One of the difficulties countered in estimating the maximum oscillation amplitude of the IRWST is that of predicting a proper reduction factor. When the prototype sparger is designed for reducing the maximum oscillation amplitude, it is essential that the number of holes be in proper perforations with an area equivalent to that of the single-hole sparger. To examine perforations in the SDVS multi-hole sparger, the area of one hole of the multi-hole sparger is compared to that of the equivalent single-hole sparger. The area ratios of the multi-hole spargers in Figure 3.16 are 0.25 and 0.10, respectively. Actually, the area ratio of the SDVS multi-hole sparger is designed not to exceed 0.005. We anticipate the SDVS multi-hole sparger to be highly perforated. If we use the reduction factor from the test, it will be a remarkably conserved value. Before applying Equation (4.1) to the prototype, the following two conditions should be met: (1) Using orifices or flow restriction device in a scaled down test facility, the requirement for the friction and form loss can be met. (2) If the source pressure is the same thermodynamic conditions as the scaled-down test, the density ratio of source steam to water can be directly applied to estimate the maximum oscillation amplitude of the SDVS multi-hole sparger. Multiplying the maximum oscillation amplitude from Equation (4.1) by an applicable reduction factor, the maximum amplitude of pressure oscillation in the prototype tank can be estimated.

6. Conclusions

A scaling methodology has been presented leading to identification of the condensation

oscillation phenomena and to the design of a scaled-down test facility of the IRWST. The key scaling parameters correlated with the maximum amplitude of condensation oscillation were found. The conclusions were as follows:

- (1) Each scaling parameter was ranked according to its importance. The similarity requirements for each scaling number were evaluated.
- (2) The key scaling parameters were flow restriction coefficient, steam cavity volume, discharge hole area, and density ratio of source steam to water.
- (3) The minimum water volume should be secured to preserve the scaling similarity and the layer thickness was equal to the maximum length of the steam cavity formed in the single-hole sparger steam jetting.
- (4) A reduction factor was introduced for estimating the oscillation amplitude of the multi-hole sparger and decreased with increases of the number of holes and the mass flux.

References

1. T. M. Su, Suppression-Tank Temperature Limits for BWR Containments, NUREG-0783, 1981.
2. C. K. Chan & C. K. B. Lee, A Regime Map for Direct Contact Condensation, *Int J. Multiphase Flow*, Vol. 8, No. 1, pp. 11-20, 1982.
3. Izuo AYA *et al.*, Pressure and Fluid Oscillation in Vent System due to Steam Condensation, (I), *Journal of Nuclear Science and Technology*, Vol. 17, pp. 499-515, 1980.
4. Izuo AYA *et al.*, Pressure and Fluid Oscillation in Vent System due to Steam Condensation, (II), *Journal of Nuclear Science and Technology*, Vol. 20, pp. 213-227, 1983.
5. Claudio Damasio, *et al.*, Experimental Study on the Unstable Direct Contact Condensation Regimes, *Proceedings of ANS-ASME-NRC International Topical Meeting on Nuclear Reactor Thermal Hydraulics*, October, 1985.
6. P. Hawtin *et al.*, On the Collapse of Water Vapour Cavities in a Bubble Analogue Apparatus, *Chemical Engineering Science*, Vol. 25, pp. 1197-1209, 1970.
7. S. M. Bhavaraju, The Design of Gas Sparged Devices for Viscous Liquid Systems, *AIChE Journal*, Vol.24, No.3, pp. 454-466, 1978.
8. Motoaki UTAMURA, Pressure Oscillation Accompanying Steam Discharge into Subcooled Liquid Tank, *Bulletin of JSME*, Vol. 29, No. 258, 1986.
9. S. Fukuda, Pressure Variations due to Vapor Condensation in Liquid, (II) Phenomena at Larger Vapor Mass Flow Flux, *J. of JNS*, Vol.24, No. 6, pp. 466-474, 1982.
10. Jung-Hoon Chun, Scaling Laws & Rate Correlations for Steam Condensation on Turbulent Water, MIT dissertation, 1983.
11. Andeen G. B. & Marks, J. S., Analysis and Testing of Steam Chugging in Pressure Systems, EPRI Report NP-908, 1978.
12. Tanks, *Nuclear Engineering and Design*, Volume 85, pp. 353-362, 1985.

Table 2.1 Scaling ratios for the test facility

Scaling ratio	Test facility
Steam cavity	1 : N_3
Pipe run	1 : $N_2 \cdot N_3$
Steam generator	1 : $N_1 \cdot N_2 \cdot N_3$

Table 2.2 Results of the scaling methodology

Equations		Characteristic time constants	Time constant scaling parameters	Similarity requirements
Mass	Steam Generator	$\tau_{SG} = \frac{\rho_s V_{SG}}{W_{SG}}$	$[N_{\tau_{SG}}]_R = \left[\frac{\tau_{SG}}{\tau_o} \right]_R = \frac{1}{N_1 N_2 N_3} \cdot \left[\frac{V_{SG}}{V_o} \right]_R$	$[N_{\tau_{SG}}]_R = 1$
	Pipe run	$\tau_{pipe} = \frac{\rho_s V_{pipe}}{W_{pipe}}$	$[N_{\tau_{pipe}}]_R = \left[\frac{\tau_{pipe}}{\tau_o} \right]_R = \frac{1}{N_2 N_3} \cdot \left[\frac{V_{pipe}}{V_o} \right]_R$	$[N_{\tau_{pipe}}]_R = 1$
	Steam cavity	$\tau_{sc} = \frac{\rho_s V_{sc}}{W_{sc}}$	$[N_{\tau_{sc}}]_R = \left[\frac{\tau_{sc}}{\tau_o} \right]_R = \left[\frac{V_{sc}}{V_o} \right]_R = 1$	$[N_{\tau_{sc}}]_R = 1$
Energy	Tank	$\tau_{tank} = \frac{\rho_f V_{minimum}}{W_{tank}}$	$[N_{\tau_{tank}}]_R = \left[\frac{\tau_{tank}}{\tau_o} \right]_R = \frac{1}{N_1 N_2 N_3} \cdot \left[\frac{\rho_f V_{minimum}}{\rho_s V_{sc}} \right]_R$	$[N_{\tau_{tank}}]_R = 1$ $[N_{heat\ loss}]_R = \left[\frac{Q_{loss}}{W_o h_s} \right]_R = 1$
Momentum	Integral	$\tau_m^{integral} = \frac{IW_o}{\rho_s u_s^2}$	$[N_{\tau_m^{integral}}]_R = \left[\frac{\tau_m^{integral}}{\tau_o} \right]_R = \left[\frac{A_{system}^2 I_{system}}{V_{sc}} \right]_R = \left[\frac{V_{system}}{V_{sc}} \right]_R$	$[N_{\tau_m^{integral}}]_R = 1$ $[N_{\rho_o}]_R = \left[\frac{\delta P_o}{\rho_s u_s^2} \right]_R = 1$ $[N_{K_f}]_R = \left[\sum \frac{fL}{D} + \sum K_f \right]_R = 1$
	Steam cavity	$\tau_m^{sc} = \left(\frac{\rho_f}{\rho_s} \right)^{1/2} V_{sc}^{1/3} u_s$	$[N_{\tau_m^{sc}}]_R = \left[\left(\frac{\rho_f}{\rho_s} \right)^{1/2} \left(\frac{V_{sc}}{L_{sc}} \right)^{1/3} \right]_R = \left[\frac{\left(\frac{\rho_f}{\rho_s} \right)^{1/2} A_{hole}}{V_{sc}^{2/3}} \right]_R$	$[N_{\tau_m^{sc}}]_R = 1$ $[N_{hy}]_R = \left[\frac{\rho_f g L_{z,o}}{\rho_s u_s^2} \right]_R = 1$ $[N_{\rho_o}]_R = \left[\frac{\delta P_o}{\rho_s u_s^2} \right]_R = 1$ $[N_{K_f}]_R = \left[\sum \frac{fL}{D} + \sum K_k \right]_R = 1$

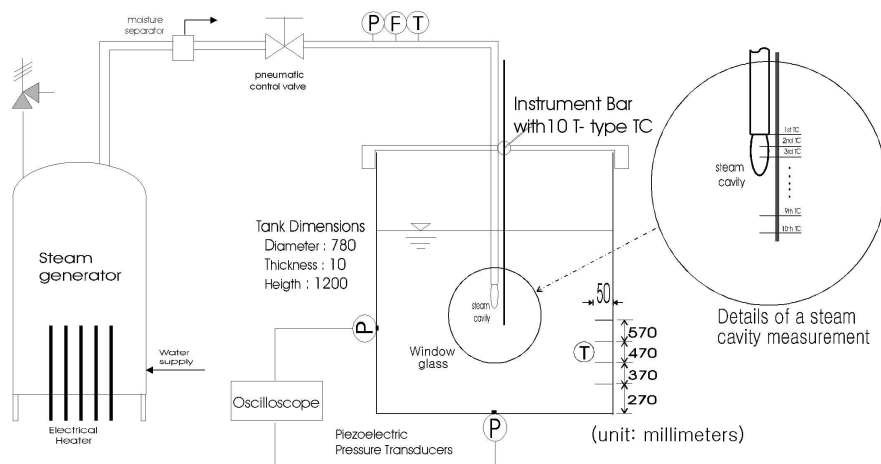


Figure 3.1 Schematic diagram of the test facility

Table 3.1 Test matrix for the single-hole sparger

Discharge hole dia. (mm)	Mass flux (kg/m ² s)	Tank water temperature (°C)	Measurement	Remark
5	200,300,400,500	30~90	-Pressure oscillation amplitude -Steam cavity axial length -Temperature profile -Oscillation Frequency	
10	70,90,150*,200**,300*,400*			* additional volumes ** degassed water effect
15.8	90***,100,150			*** tank size, degassed water, and increased volume

Note: In addition to normal tests, asterisk marks show that additional tests were performed to clarify the parametric effects on the condensation phenomenon.

Table 3.2 Test matrix for the multi-hole sparger

Discharge Hole diameter (mm)	Number of holes	Equivalent single-hole sparger (mm)	Mass flux (kg/m ² s)	Remark
3.16	10	10	90,150,400	
5	4	10	90,150,400	hole position effect

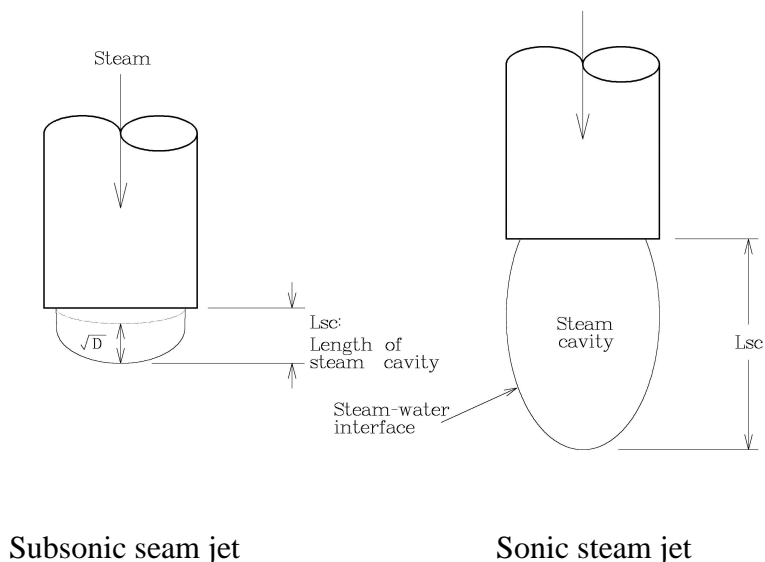
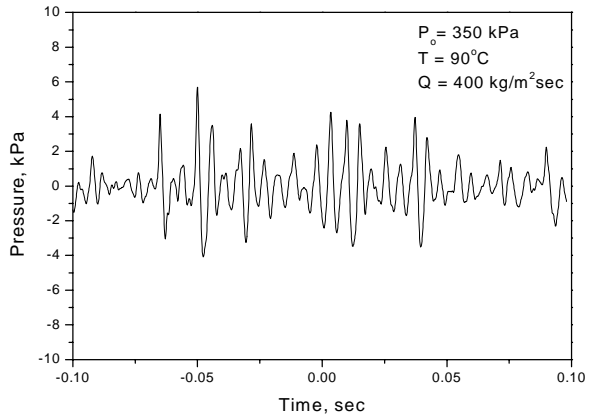
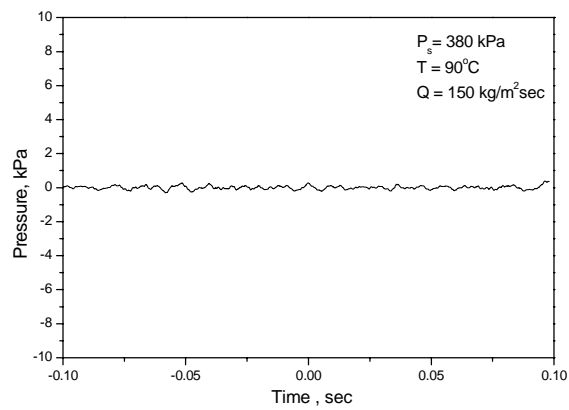
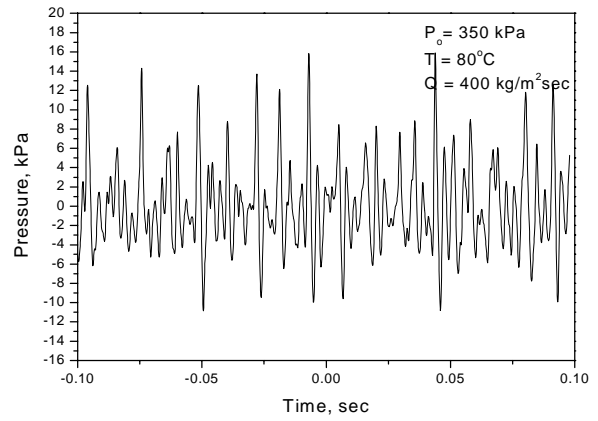
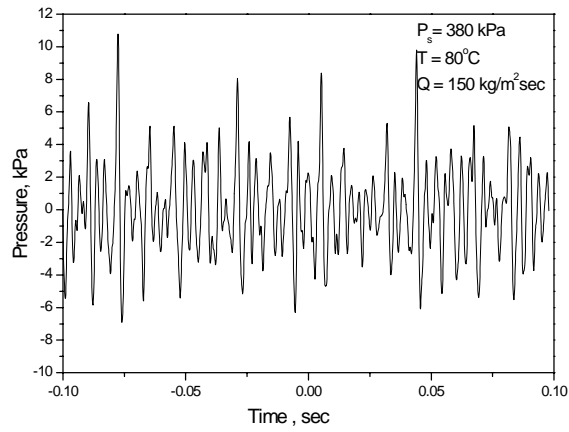
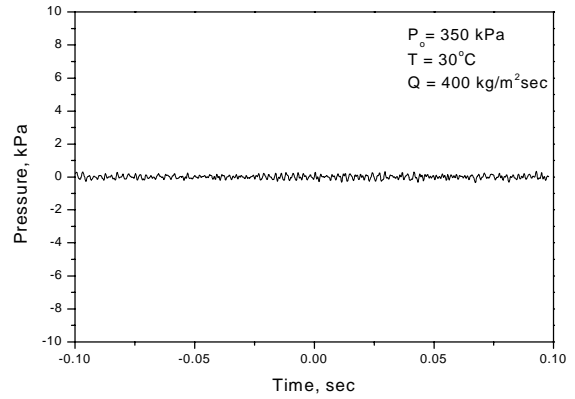
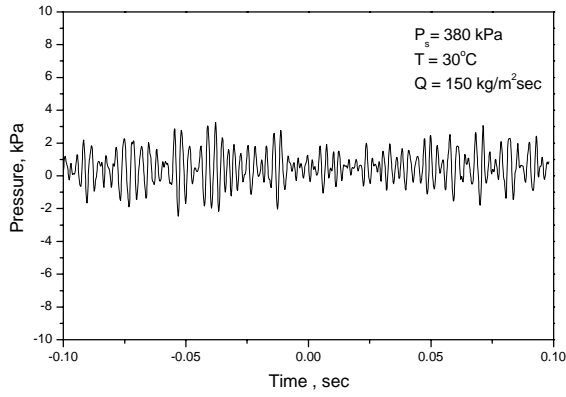


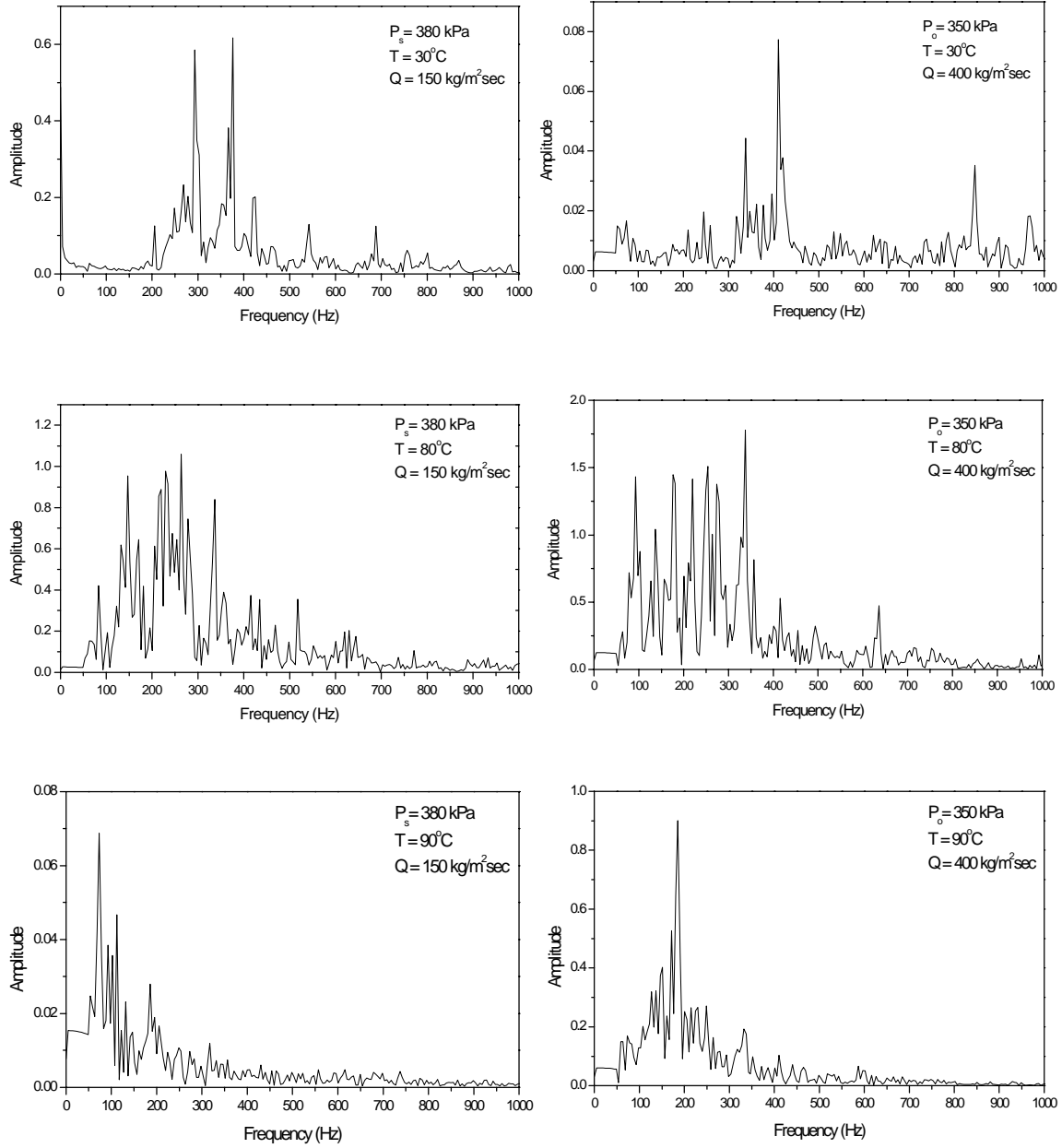
Figure 3.2 Steam cavity model



Subsonic steam jet

Sonic steam jet

Figure 3.3 Pressure time history



Subsonic steam jet

Sonic steam jet

Figure 3.4 Oscillation frequency

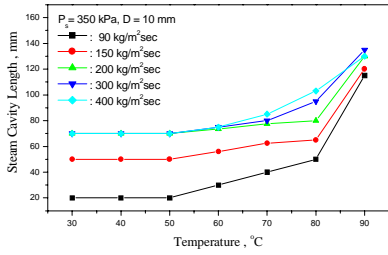


Figure 3.5 Steam cavity length

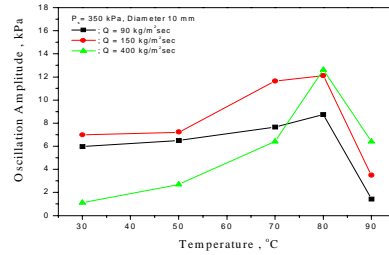
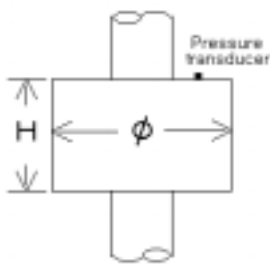


Figure 3.6 Oscillation amplitude



Type A dry well ($\phi 150 \text{ mm} \times H 150 \text{ mm}$)

Type B dry well ($\phi 480 \text{ mm} \times H 300 \text{ mm}$)

Figure 3.7 Dimensions of the dry well.

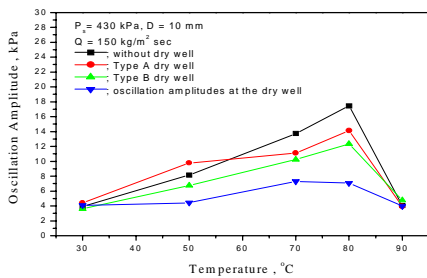


Figure 3.8 Increased volume effect of the subsonic steam jet

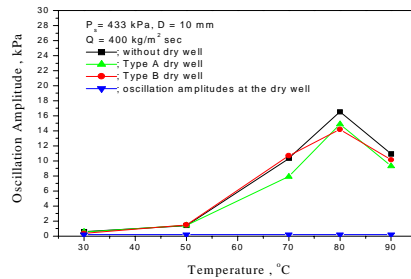


Figure 3.9 Increased volume effect of the sonic steam jet.

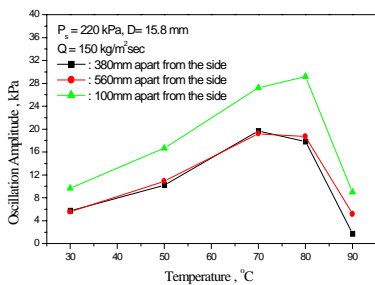


Figure 3.10 Minimum water volume effect of the single-hole sparger

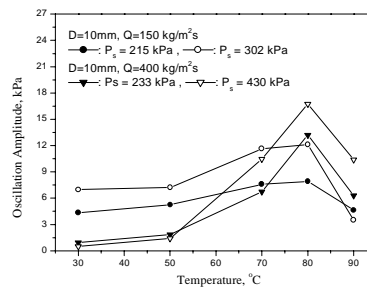


Figure 3.11 Source pressure effect

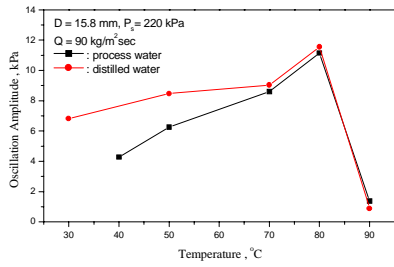


Figure 3.12 Oscillation amplitude between distilled and process water

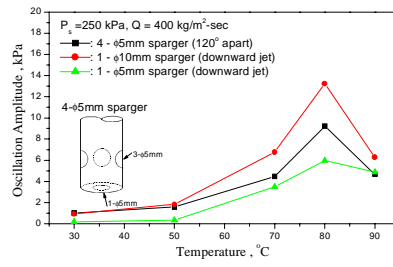


Figure 3.13 Oscillation amplitude for the multi-hole sparger

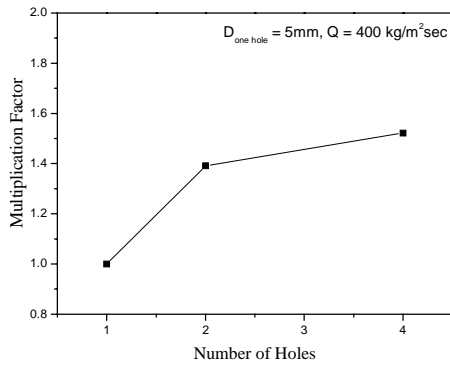


Figure 3.14 Effect of the number of holes

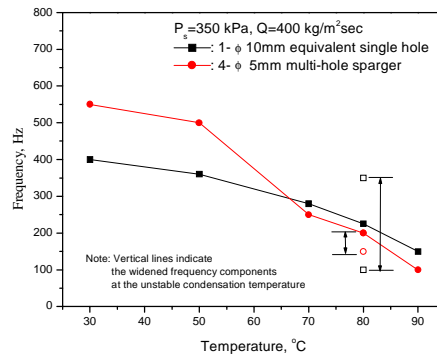


Figure 3.15 Oscillation frequency between the equivalent single- and multi-hole spargers

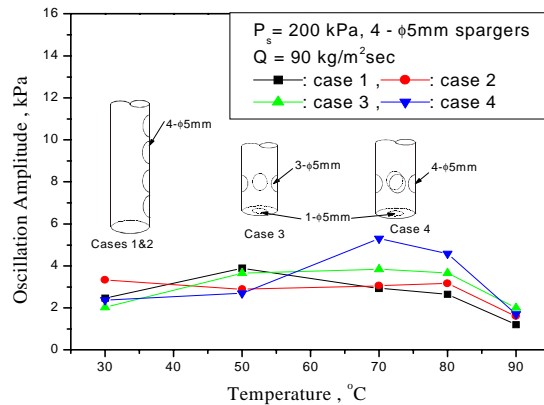


Figure 3.16 Oscillation amplitude on each separate test case.

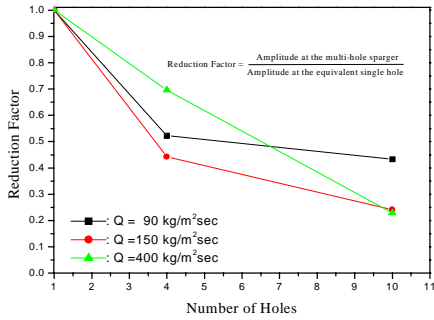


Figure 3.17 Reduction factor

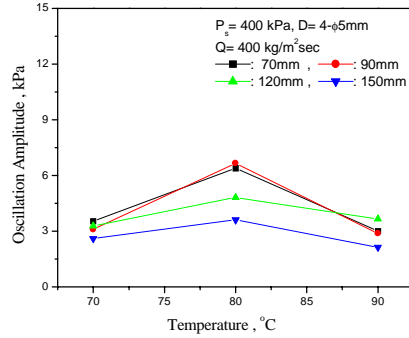


Figure 3.18 Minimum water volume effect of the multi-hole sparger

Table 4.1 Evaluation of scaling methodology

Experimental parameters*	Oscillation amplitude	Oscillation frequency	Scaling parameters	Phenomena importance
Water temperature	↑	↓	V_{sc}	High
Mass flux	↑	↑	V_{sc}	High
Increased Volume (drywell)	↓	↓	V_{system}, K_f	Medium
Discharge hole diameter	↑	↓	A_{hole}	High
Minimum water volume	↓	↑	$V_{minimum}$	Low
Source pressure	↑	↑	$P_{source}, \rho_{source}$	Medium
Degassed liquid	↑	↓	.	Low
Jetting direction	.	.	.	Low
Number of discharge hole	↓	↑	N_3	High
Submersion depth	.	.	.	Low

Note: The asterisk mark indicates an increased value of the parameters

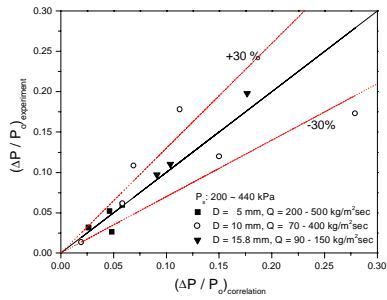


Figure 4.1 Maximum oscillation amplitude

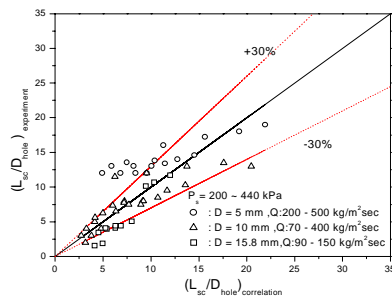


Figure 4.2 Dimensionless cavity length